Carbohydrate Polymers 289 (2022) 119415

Contents lists available at ScienceDirect

Carbohydrate Polymers

journal homepage: www.elsevier.com/locate/carbpol

Strategy to identify reduced arabinoxylo-oligosaccharides by HILIC-MS^n

Dimitrios Kouzounis, Peicheng Sun, Edwin J. Bakx, Henk A. Schols, Mirjam A. Kabel *

Laboratory of Food Chemistry, Wageningen University & Research, 6708 WG Wageningen, the Netherlands

ARTICLE INFO

Keywords:
Arabinoxylo-oligosaccharides
AXOS
HILIC-ESI-CID-MS^n
Negative ion mode
$NaBH_4$ reduction
Structural elucidation

ABSTRACT

Identification of arabinoxylo-oligosaccharides (AXOS) within complex mixtures is an ongoing analytical challenge. Here, we established a strategy based on hydrophilic interaction chromatography coupled to collision induced dissociation-mass spectrometry (HILIC-MS^n) to identify a variety of enzyme-derived AXOS structures. Oligosaccharide reduction with sodium borohydride remarkably improved chromatographic separation of isomers, and improved the recognition of oligosaccharide ends in MS-fragmentation patterns. Localization of arabinosyl substituents was facilitated by decreased intensity of Z ions relative to corresponding Y ions, when fragmentation occurred in the vicinity of substituents. Interestingly, the same B fragment ions (MS^2) from HILIC-separated AXOS isomers showed distinct MS^3 spectral fingerprints, being diagnostic for the linkage type of arabinosyl substituents. HILIC-MS^n identification of AXOS was strengthened by using specific and well-characterized arabinofuranosidases. The detailed characterization of AXOS isomers currently achieved can be applied for studying AXOS functionality in complex (biological) matrices. Overall, the present strategy contributes to the comprehensive carbohydrate sequencing.

1. Introduction

Arabinoxylan (AX) is an abundant cereal fiber in both human and animal diets. Investigating the prebiotic and immunomodulatory properties of AX and (enzymatically) derived arabinoxylo-oligosaccharides (AXOS) is of great nutritional, scientific and commercial interest (Broekaert et al., 2011; Mendis et al., 2016). Previous studies have shown that the prebiotic potential of AXOS depended on degree of polymerization (DP) and substitution pattern (Broekaert et al., 2011; Mendis et al., 2018; Rumpagaporn et al., 2015). Therefore, detailed characterization of AXOS in complex matrices may greatly improve our understanding about their bio-functionality.

In general, cereal grain AX (i.e., from wheat, maize, rye, rice) is composed of a backbone of β-(1 → 4)-linked D-xylosyl (Xyl) residues, substituted mainly by L-arabinofuranosyl (Ara) units at the *O*-2- and/or *O*-3-positions of Xyl units. To a lesser extent, 4-*O*-D-methyl-glucuronoyl and acetyl substituents occur, and a part of the Ara units might be further *O*-5-substituted by feruloyl units (Fauré et al., 2009; Izydorczyk & Biliaderis, 1995). Cereal grains present diverse AX populations, primarily due to variation in the type and distribution of Ara substituents over the AX backbone (Gruppen et al., 1993b; Saulnier et al., 2007; Vinkx & Delcour, 1996; Wang et al., 2020). Consequently, the corresponding (enzyme-derived) AXOS mixtures contain a range of differently substituted structures.

Although oligosaccharide identification has considerably improved in the last decades (Kamerling & Gerwig, 2007; Nagy et al., 2017; Wang et al., 2021), detailed identification of AXOS in mixtures remains an ongoing analytical challenge due to the aforementioned complexity. High Performance Anion Exchange Chromatography (HPAEC) has been shown to provide valuable information regarding the oligosaccharide composition of enzymatic (A)XOS digests (Gruppen et al., 1993a; McCleary et al., 2015; Mechelke et al., 2017; Pastell et al., 2008). However, scarcely available standards and low compatibility with mass spectrometric techniques, due to the high salt concentration of eluents, hamper the identification of unknown oligosaccharides by HPAEC (Mechelke et al., 2017; Nagy et al., 2017). AXOS purified from enzymatic digests were subjected to nuclear magnetic resonance (^{1}H NMR) spectroscopy to accurately determine the position and linkage type of

Abbreviations: AX, arabinoxylan; AXOS, arabinoxylo-oligosaccharides; XOS, xylo-oligosaccharides; Ara, arabinosyl substituents of AX/AXOS; Xyl, xylosyl residues; GH, glycosyl hydrolase; Abf, arabinofuranosidase; $NaBH_4$, sodium borohydride; HPAEC-PAD, high performance anion exchange chromatography with pulsed amperometric detection; HILIC, hydrophilic interaction liquid chromatography; ESI-CID, electrospray ionization - collision induced dissociation; MS^n, tandem mass spectrometry.

* Corresponding author.
E-mail address: mirjam.kabel@wur.nl (M.A. Kabel).

https://doi.org/10.1016/j.carbpol.2022.119415
Received 18 January 2022; Received in revised form 23 March 2022; Accepted 23 March 2022
Available online 28 March 2022

Ara substituents (Biely et al., 1997; Gruppen et al., 1992; Hoffmann et al., 1991; Pastell et al., 2008). Still, ^{1}H NMR analysis requires high purity and amount of analytes (Kiely & Hickey, 2022), which complicates the analysis of (minorly present) AXOS from complex biological matrices. Next to ^{1}H NMR, direct infusion mass spectrometry (MS^n), has been widely used for AXOS structural analysis (Matamoros Fernández et al., 2004; Mazumder & York, 2010; Quéméner et al., 2006; Wang et al., 2021). In specific, hyphenation of MS^n to normal phase and reverse phase liquid chromatography (LC-MS^n) further progressed AXOS characterization (Bowman et al., 2012; Maslen et al., 2007). Still, chromatographic resolution was not sufficient to address AXOS identification in complex biological mixtures. Hydrophilic interaction liquid chromatography (HILIC) was recently reviewed to exhibit increased selectivity for glycan analysis compared to reverse phase chromatography, and higher compatibility with MS compared to normal phase chromatography (Nagy et al., 2017). HILIC coupled to MS has been assessed to separate and characterize in vitro-generated AXOS, human milk oligosaccharides, as well as cello-, galacto-, manno-, arabino- and pectic oligosaccharides mixtures (Demuth et al., 2020; Hernández-Hernández et al., 2012; Juvonen et al., 2019; Leijdekkers et al., 2011; Remoroza et al., 2018; Sun et al., 2020). Furthermore, the characterization of alginate-oligosaccharides in fecal samples by HILIC-MS (Jonathan et al., 2013) demonstrated the potential of HILIC-based approaches to separate and identify oligosaccharides present in complex biological matrices. Still, further research is warranted to improve HILIC separation and MS-based identification of AXOS isomers present in mixtures.

The chromatographic resolution of α- and β-anomers of oligosaccharides in LC, including HILIC, has been shown to result in signal loss and peak broadening (Churms, 2002; Schumacher & Kroh, 1995). The latter can be overcome by reducing oligosaccharides, for example with sodium borohydride ($NaBH_4$) (Abdel-Akher et al., 1951; York et al., 1996). Such reduction has been shown to result in better HILIC separation for cello-oligosaccharide mixtures with increased signal intensities, and allows the discrimination in MS of fragment ions originating from either the non-reducing or reduced end (Domon & Costello, 1988; Sun et al., 2020; Vierhuis et al., 2001). So far, to the best of our knowledge, chromatographic resolution and MS fragmentation patterns of $NaBH_4$-reduced (A)XOS subjected to HILIC-MS^n have not been studied.

Hence, the present study aimed at developing a strategy to characterize individual (A)XOS present in complex mixtures formed during arabinoxylan depolymerization by *endo*-xylanases. For that, AXOS mixtures were further treated with arabinofuranosidases and were reduced by $NaBH_4$, prior to their HILIC-MS^n analysis. Hereto, it was hypothesized that structurally different $NaBH_4$-reduced (A)XOS show chromatographic resolution in HILIC and exhibit distinct MS fragmentation patterns. The principles on which this strategy is based are considered compatible with the analytical needs for the structural elucidation of other types of polysaccharides.

2. Materials and methods

2.1. Materials

Wheat flour arabinoxylan (medium viscosity; WAX), linear XOS (DP 2–6; X_2-X_6), branched AXOS standards (XA^3XX, XA^2XX & XA^3XX mixture, $A^{2+3}XX$), GH10 endo-1,4-β-xylanase from *Thermotoga maritima* (Xyn_10), GH43 α-arabinofuranosidase from *Bifidobacterium adolescentis* (Abf_43) and GH51 α-arabinofuranosidase from *Aspergillus niger* (Abf_51) were obtained from Megazyme (Bray, Ireland). A commercial enzyme preparation (HX) enriched in GH11 endo-1,4-β-xylanase from *Trichoderma citrinoviride* was provided by Huvepharma NV (Berchem, Belgium). In AXOS abbreviations, unsubstituted xylosyl residues are annotated as X, while xylosyl residues substituted at *O*-2, *O*-3 or at both *O*-2 and *O*-3 positions by arabinosyl units are annotated as A^2, A^3 and A^{2+3}, respectively, according to Fauré et al. (2009).

2.2. In vitro production of arabinoxylo-oligosaccharides (AXOS)

WAX (5.5 mg/mL) was dissolved in 50 mM sodium acetate (NaOAc) buffer (pH 5.0). Next, 4.55 mL WAX solution was transferred in a 15 mL tube, and 455 μL of HX or Xyn_10 solution pre-diluted in the same NaOAc buffer was added to start the incubations. The enzyme doses used were chosen to result in total or 'end-point' degradation of WAX. Incubations were carried out at 40 °C overnight followed by enzyme inactivation at 99 °C for 15 min. Supernatants (e.g., AXOS mixtures) were analyzed with HPAEC-PAD (10 times diluted), and after reduction (see Section 2.4) with HILIC-ESI-CID-MS^n.

2.3. Enzymatic fingerprinting of arabinosyl substituents in AXOS

Two AXOS mixtures obtained (see Section 2.2) by using the two distinct *endo*-xylanases were subsequently treated with Abf_43, Abf_51 and a combination thereof (Abf_43/Abf_51). GH51 Abfs release single *O*-2- or *O*-3-linked arabinosyl substitutions (reviewed by Lagaert et al., 2014), while Abf_43 only releases the *O*-3 arabinosyl from a disubstituted Xyl moiety (Sørensen et al., 2006; Van den Broek et al., 2005). Although the Abf_51 currently used was previously shown to be also active toward disubstituted AXOS, especially $A^{2+3}XX$ (Koutaniemi & Tenkanen, 2016), in our research, only a very minor amount of $A^{2+3}XX$ was degraded after 8 h and current experimental conditions, as shown by HPAEC (see Fig. S1). Aliquots (500 μL) of the AXOS mixtures were transferred in clean reaction tubes and were mixed with 480 μL or 460 μL 50 mM sodium acetate buffer (pH 5.0) for single or combined Abf incubations, respectively. Next, 20 μL of Abf_43 and/or Abf_51 solution was added to achieve a final dosing of 0.1 U/mL. The samples, alongside controls with no Abf added, were incubated at 40 °C for 8 h, followed by enzyme inactivation at 99 °C for 15 min. Oligosaccharide and Abf digests were analyzed with HPAEC-PAD (10 times diluted), and after reduction with HILIC-ESI-CID-MS^n.

2.4. Reduction of oligosaccharides

Aliquots (200 μL) of DP2–6 XOS mixture (1 mg/mL each), $A^{2+3}XX$ (1 mg/mL), A^2XX (1 mg/mL; see Supplementary information), XA^3XX (1 mg/mL), XA^2XX/XA^3XX (2 mg/mL), AXOS mixtures (1 mg/mL; see Section 2.2) and AXOS mixtures digested with Abfs (1 mg/mL; see Section 2.3) were reduced with 200 μL 0.5 M $NaBH_4$ solution in 1 M NH_4OH at room temperature for 4 h. The reaction was stopped by addition of 50 μL acetic acid and was followed by sample clean up on Supelclean™ ENVI-Carb™ solid phase extraction (SPE) cartridges (250 mg, Sigma Aldrich, St. Louis, MO, USA). The cartridges were activated with 80% (v/v) acetonitrile (ACN; Biosolve, Valkenswaard, The Netherlands) containing 0.1% (v/v) trifluoroacetic acid (TFA; Sigma Aldrich) and conditioned with water. Samples were loaded on the cartridges and washed with water. Analytes eluting with 40% (v/v) ACN containing 0.1% (v/v) TFA were collected and dried by evaporation. The dried analytes were redissolved in 400 μL 50% ACN prior to their HILIC-ESI-CID-MS^n analysis.

2.5. Separation and identification of reduced AXOS with HILIC-ESI-CID-MS^n

Separation and identification of individual AXOS in mixtures was performed by hydrophilic interaction chromatography - electrospray ionization - collision induced dissociation - tandem mass spectrometry (HILIC-ESI-CID-MS^n) using a previously described method (Sun et al., 2020), with modifications. The analysis was performed on a Vanquish UHPLC system (Thermo Fisher Scientific, Waltham, MA, USA) equipped with an Acquity UPLC BEH Amide column (Waters, Millford, MA, USA; 1.7 μm, 2.1 mm ID × 150 mm) and a VanGuard pre-column (Waters; 1.7

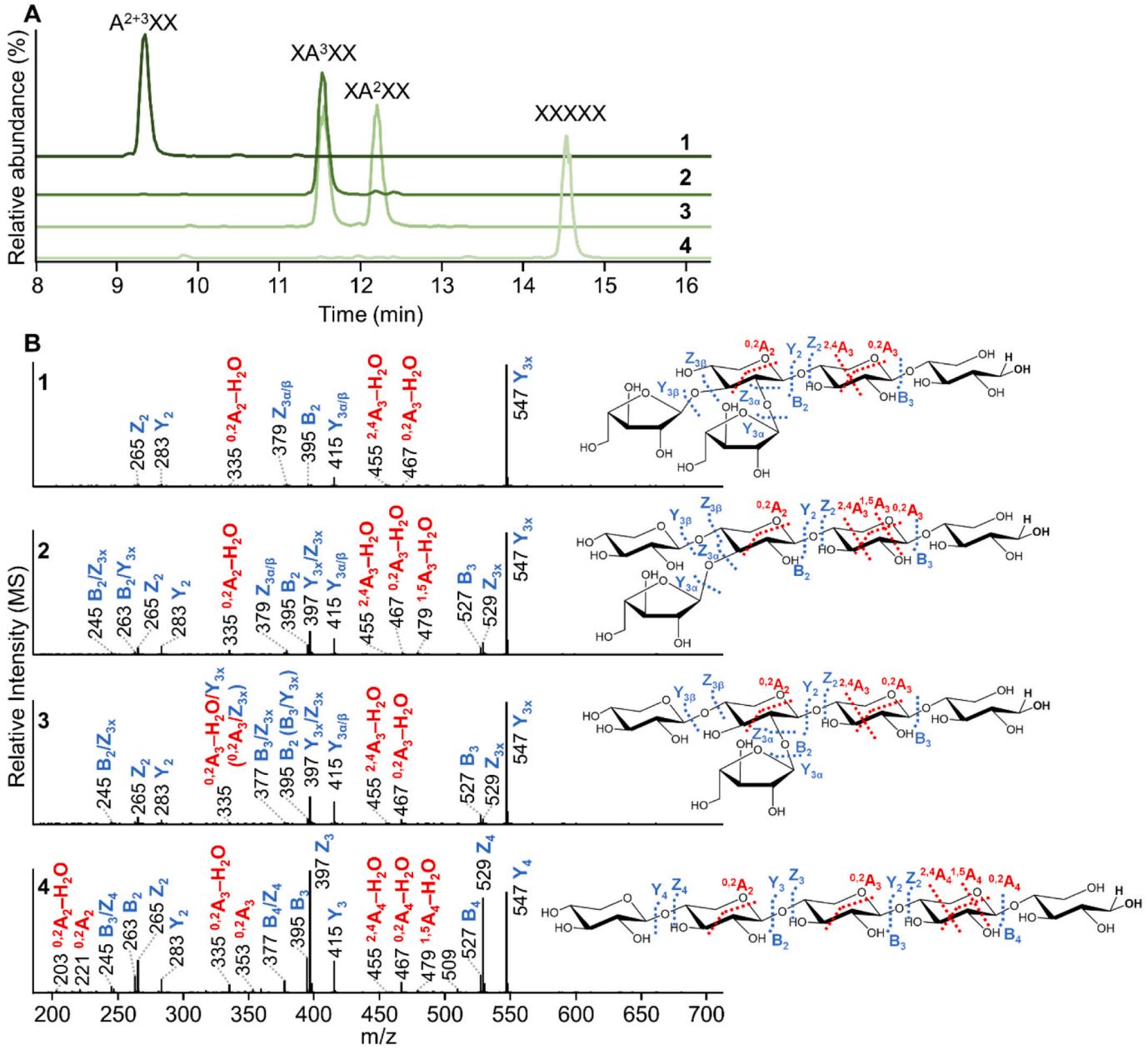

Fig. 1. HILIC-MS extracted ion chromatograms (A) of four $NaBH_4$-reduced DP5 (*m/z* 679; $[M–H]^-$) isomers: $A^{2+3}XX$ (1), XA^3XX(2), XA^2XX (3) and X_5 (4). Negative ion mode CID-MS^2 spectra (B) of eluted isomers 1–4; average spectra across the chromatographic peaks. The fragments are annotated according to Domon and Costello (1988) and Juvonen et al. (2019). Blue: glycosidic linkage fragments; Red: cross-ring fragments; /: double cleavage; x: α or β antennae. Alternative fragments are presented in brackets.

μm, 2.1 mm ID × 5 mm). The column temperature was set at 35 °C and the flow rate was 0.45 mL/min; injection volume was 1 μL. Water (A) and ACN (B), both containing 0.1% (v/v) formic acid (FA) (all solvents were UHPLC-grade; Biosolve), were used as mobile phases. The separation was performed by using the following elution profile: 0–2 min at 82% B (isocratic), 2–32 min from 82% to 71% B (linear gradient), 32–32.5 min from 71% to 42% B (linear), 32.5–39 min at 42% B (isocratic), 39–40 min from 42% to 82% B (linear) and 40–50 min at 82% B (isocratic). Oligosaccharide mass (*m/z*) was on-line detected with an LTQ Velos Pro mass spectrometer (Thermo Fisher Scientific) operated in a negative ion mode. The mass spectrometer was equipped with a heated ESI probe, and was run at three modes: Full MS, MS^2 on selected MS ions, and MS^3 on selected MS^2 ions. Ion selection was different for DP 3, 4, 5, 6 and 7 oligosaccharides (Table S1), and each DP series was analyzed in separate runs. The settings used were: source heater temperature 425 °C, capillary temperature 263 °C, sheath gas flow 50 units and source voltage 2.5 kV. MS^2 scanning was performed at *m/z* range 150–1200: CID with normalized collision energy set at 40%, activation Q of 0.25 and activation time of 10 ms. The *m/z* range of MS^3 scan events depended on the *m/z* value of the daughter ion. The CID was set at 35%, while all other parameters were similar to MS^2 scanning. Mass spectrometric data were processed by using Xcalibur 2.2 software (Thermo Fisher Scientific).

3. Results and discussion

3.1. Separation and identification of reduced, isomeric AXOS standards

The aim of this research was to develop a strategy for AXOS identification in complex mixtures, making use of HILIC-MS^n. It was

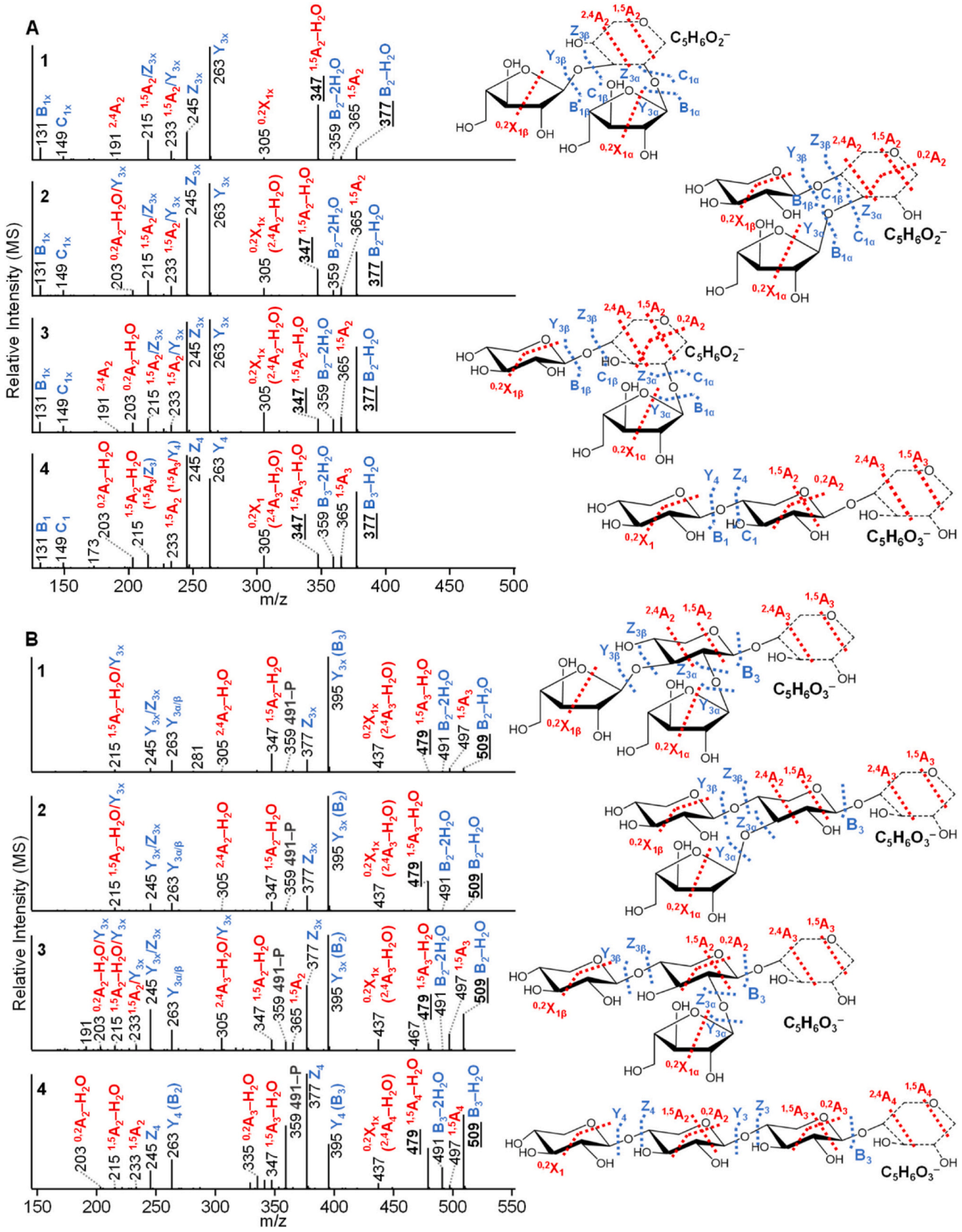

Fig. 2. Negative ion mode CID-MS^3 spectra of *m/z* 679 → 395 $[M–H]^-$ (A) and *m/z* 679 → 527 $[M–H]^-$ (B) corresponding to $A^{2+3}XX$ (1), XA^3XX (2), XA^2XX (3) and X_5 (4) (MS^2; see Fig. 1). The fragments are annotated according to Domon and Costello (1988) and Juvonen et al. (2019). Blue: glycosidic fragments; Red: cross-ring fragments; /: double cleavage; x: α or β antennae. Alternative fragments are presented in brackets. The precise structure of the newly formed end of B fragment ions is unknown as it may undergo several rearrangements (dashed ring), hence corresponding MS^3-ring-fragments have been annotated tentatively.

hypothesized that reduction of the oligosaccharides would not only improve chromatographic resolution, but would also aid in their MS-based identification, as has been suggested for other types of oligosaccharides (Bennett & Olesik, 2017; Vierhuis et al., 2001; York et al., 1996). First, the elution and fragmentation patterns of reduced, standard (A)XOS all having a DP of 5 ($A^{2+3}XX$, XA^3XX, XA^2XX, X_5) were investigated (Figs. 1, 2), before delving into complex AXOS mixtures. The overall separation and resolution of reduced DP 5 isomers was enormously improved (Fig. 1A) in comparison to that of underivatized (A)XOS (Fig. S2). The reduced (A)XOS isomers eluted in the following order: $A^{2+3}XX$, XA^3XX, XA^2XX and X5 (Fig. 1A). Interestingly, the observed shorter retention times of reduced AXOS compared to the linear (reduced) counterpart (e.g., X_5), provides a first indication of arabinosyl substitution when specific analytical standards are not available.

Full-scan MS mode (data not shown) indicated that oligosaccharides were present in a single-charged, deprotonated state ($[M–H]^-$) or as deprotonated formate adducts ($[M+FA–H]^-$). The $[M–H]^-$ products were preferred for further MS analysis, because fragmentation of $[M+FA–H]^-$ products was either not obtained or resulted in complex spectra with various formate-adducted fragments, as was also observed by Sun et al. (2020) for cello-oligosaccharides.

The obtained fragmentation spectra were annotated according to the nomenclature proposed by Domon and Costello (1988). MS^2 analysis (Fig. 1B) revealed that for all separated reduced standard DP 5 AXOS (Fig. 1A), Y ($Y_{4\text{-}2}$: *m/z* 547, 415, 283), Z ($Z_{4\text{-}2}$: *m/z* 529, 397, 265) and B ($B_{4\text{-}2}$: *m/z* 527, 395, 263) ions were the main fragments, while C ions (C_3: *m/z* 413, C_2: *m/z* 281) were only visible at highest zoom levels (not shown). Z ions were predominant for X_5, but less abundant for Ara-substituted isomers (Fig. 1). In particular, the abundance of Z_3 and Z_2 was lower in $A^{2+3}XX$ compared to XA^3XX and XA^2XX. The lower abundance of C ions in negative ion mode MS^2 has not been previously observed for underivatized oligosaccharides, such as AXOS and cello-oligosaccharides (Juvonen et al., 2019; Quéméner et al., 2006; Sun et al., 2020). More explicitly, C ions occurring from the reducing end, have been previously described as integral diagnostic fragments for such underivatized AXOS structures (Juvonen et al., 2019; Quéméner et al., 2006). Most likely, reduction resulted in less stable C ions compared to Y, Z and B ions. This observation is in line with previous studies reporting the decrease in C ion abundance after reduction of mucin-derived oligosaccharides, cello-oligosaccharides, and galacto-oligosaccharides (Doohan et al., 2011; Logtenberg et al., 2020; Sun et al., 2020). Cross-ring fragments $^{0,2}A_n$ and $^{2,4}A_n$ were observed at relatively low abundances (Fig. 1B), mainly with further loss of water (e.g., $^{0,2}A_{4(3)}$–H_2O: *m/z* 467, $^{0,2}A_{3(2)}$–H_2O: *m/z* 335). Nevertheless, these two cross-ring fragment types have been proven to be important indicators of the β-(1 → 4) linkages between xylosyl backbone residues (Quéméner et al., 2006). Furthermore, double cleavages involving B and Y or Z glycosidic ions, as well as $Y_{3\alpha}/Y_{3\beta}$, $Z_{3\alpha}/Z_{3\beta}$, Y_{3x}/Z_{3x} double cleavages were observed (Fig. 1), in line with MS^2 fragmentation spectra of underivatized oligosaccharides in previous reports (Bauer, 2012; Domon & Costello, 1988; Juvonen et al., 2019). Additional double cleavages involving glycosidic and cross-ring fragments ($^{0,2}A_n$/Y ($^{0,2}A_n$–H_2O/Z)) currently observed have been also reported for underivatized AXOS (Juvonen et al., 2019). For example, *m/z* 335 was observed in all four isomers (Fig. 1), and represented a cross-ring cleavage ($^{0,2}A_{2(3)}$–H_2O) in XA^3XX and X_5. Yet, the formation of *m/z* 335 in XA^2XX and $A^{2+3}XX$ could not be explained by $^{0,2}A_x$ cleavage alone, and might have resulted from double cleavage that involved the loss of *O*-2-linked Ara. The formation of such double cleavage fragment ions is not uncommon (Bauer, 2012; Domon & Costello, 1988; Rodrigues et al., 2007), but impedes conclusive identification of the four isomers based on their MS^2 spectra.

Therefore, relevant Y and B fragment ions (MS^2) were further investigated by MS^3. To that end, MS^3 analysis of $Y_{3(4)}$ (*m/z* 547) (Fig. S3), $B_{3(4)}$ (*m/z* 527) and $B_{2(3)}$ (*m/z* 395) (Fig. 2) was carried out. MS^3 analysis of *m/z* 679 → 547 ion across all four DP 5 isomers mainly showed B and Y fragments, while the formation of Z_3 (*m/z* 397) was more restricted in $A^{2+3}XX$ than in XA^3XX and XA^2XX (Fig. S3). The latter confirmed the MS^2 analysis of AXOS structures (Fig. 1), pointing out that Z ions were less favored in the vicinity of Ara substituents. Conversely, the corresponding MS^3 spectra of *m/z* 679 → 547 ions for XA^3XX and XA^2XX resembled that of X_5 (Fig. S3). This observation indicated the loss in MS^3 of Ara instead of the terminal xylosyl moiety, from both MS^2 ions having the same *m/z* value.

In MS^3, the spectra of all isomers in the case of *m/z* 679 → 395 and *m/z* 679 → 527 were dominated by B, Y and Z ions, while $^{1,5}A$ and $^{2,4}A$ ions were also present (Fig. 2). In particular, isomers presented distinct MS^3 spectra for *m/z* 679 → 395, mainly differing in relative intensities of *m/z* 377, 359, 365 and 347 ions (Fig. 2A). The ions *m/z* 377 and *m/z* 359

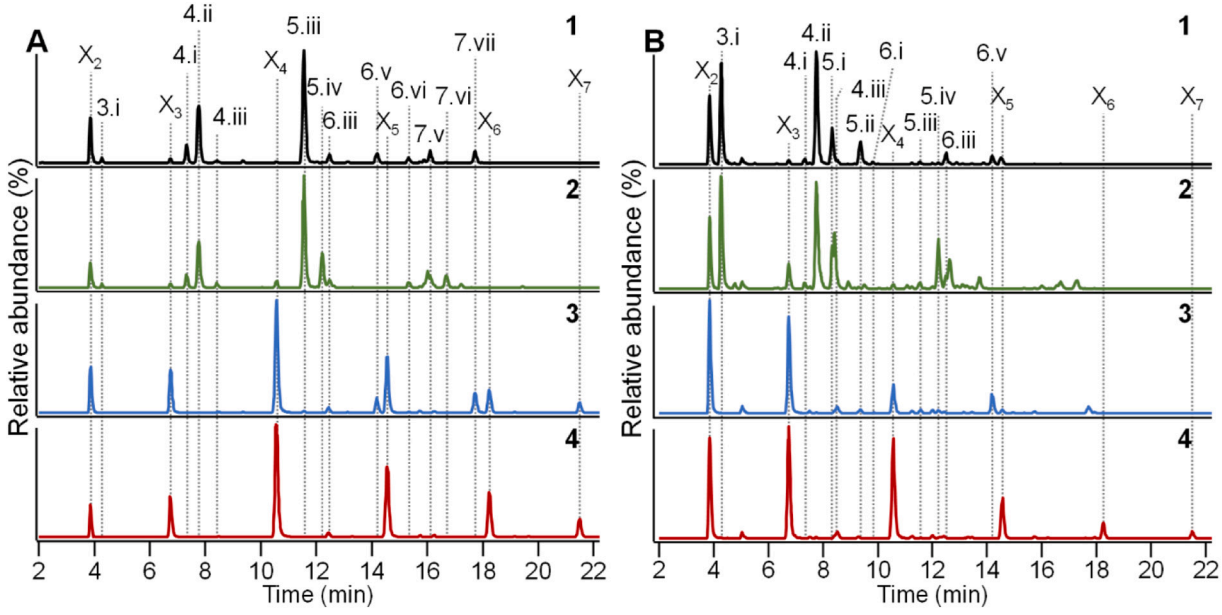

Fig. 3. HILIC-MS extracted ion chromatograms of $NaBH_4$-reduced AXOS and XOS from WAX digested by HX (A.1) and Xyn_10 (B.1). Subsequent digestions with Abf_43 (2), Abf_51 (3) or Abf_43/Abf_51 combination (4), see Table 1 for explanation of coded peaks.

Table 1
Overview of (A)XOS isomers DP 2–7 detected by HILIC-ESI-CID-MS^n. The *m/z* [M–H]$^-$, number of isomers (*n*), code, retention time (RT), relative abundance, characteristic MS^2 and MS^3 ions, diagnostic MS^3 ion ratio and the resolved structures of (A)XOS are included.

m/z [M-H]$^-$ (DP)	Iso-mers (*n*)	Code	RT (min) (ΔRT, min)[a]	Relative abundance[b] (%)		Characteristic fragment ions (*m/z*)[c]	MS^2 fragment ion (*m/z*)			Structure
							263[d]	*395*[d]	*527*[d]	
				HX	Xyn_10		Diagnostic MS^3 ion ratio[e]			
283 (2)	1	X_2	3.9	12.0	14.8	–	–	–	–	XX[g]
415 (3)	2	3.i	4.3 (2.5)	1.3	24.4	MS^2: 283, 265, 263, 221	40.9	–	–	A^3X
		X_3	6.8	1.2	1.0	MS^3: **263** (245, 215, 173, 131, 113)	0.4	–	–	XXX[g]
547 (4)	4	4.i	7.3 (3.3)	5.6	1.3	MS^2: 415, 397	–	9.6	–	A^3XX
		4.ii	7.8 (2.8)	20.5	31.1	MS^3: **395** (377, 347, 305, 263,245)	–	0.6	–	XA^3X
		4.iii	8.4 (2.2)	1.0	1.0		–	0.1	–	A^2XX[g]
		X_4	10.6	0.4	–		–	0.2	–	XXXX[g]
679 (5)	5	5.i	8.3 (6.3)	–	8.3	MS^2: 547, 529	–	9.7	–	A^3A^3X[f]
		5.ii	9.3 (5.3)	0.7	6.6	MS^3: **547** (415,397), **527** (509,479, 437, 395, 377)	–	4.7	0.3	$A^{2+3}XX$[g]
		5.iii	11.5 (3.1)	37.8	0.6	**395** (same as DP 4)	–	0.6	152	XA^3XX[g]
		5.iv	12.2 (2.4)	–	0.4		–	0.2	0.2	XA^2XX[g]
		X_5	14.6	–	–		–	0.2	0.5	XXXXX[g]
811 (6)	9	6.i	9.8 (8.4)	–	0.4	MS^2: 679, 661	–	–	–	$A^{2+3}A^3X$[f]
		6.ii	12.0 (6.2)	–	0.3	MS^3:**679** (547, 529), **547** (415, 397), **527** (same as DP 5)	–	–	1.2	Mlt_{Sin}[h]
		6.iii	12.5 (5.7)	3.3	3.2		–	–	20.8	XA^3A^3X[f]
		6.iv	13.1 (5.1)	0.5	0.3		–	–	2.4	–
		6.v	14.2 (4.0)	3.8	2.5		–	–	1.4	$XA^{2+3}XX$
		6.vi	15.3 (2.9)	1.9	–		–	–	1.7	XA^3XXX
		6.vii	15.7 (2.5)	0.2	0.1		–	–	7.2	XXA^3XX
		6. viii	16.0 (2.2)	–	0.1		–	–	0.7	XA^2XXX
		X_6	18.2	–	–		–	–	0.6	XXXXXX[g]
943 (7)	7	7.i	12.9 (8.6)	–	0.5	MS^2: 811,793	–	–	–	Mlt_{Sin}[h]
		7.ii	13.9 (7.6)	–	0.5	MS^3: **811** (679, 661), **679** (same as DP 6), **527** (same as DP 5)	–	–	2.0	Mlt_{mix}[h]
		7.iii	14.5 (7.0)	–	2.2		–	–	0.9	Mlt_{mix}[h]
		7.iv	15.9 (5.6)	0.8	–		–	–	2.9	Mlt_{Sin}[h]
		7.v	16.1 (5.4)	4.1	–		–	–	3.7	XA^3A^3XX[f]
		7.vi	16.6 (4.9)	0.3	0.2		–	–	–	–
		7.vii	17.7 (3.7)	4.3	0.1		–	–	0.9	$XA^{2+3}XXX$
		X_7	21.5	–	–		–	–	0.6	XXXXXXX

[a] Relative retention time (ΔRT) of AXOS compared to linear XOS of the same DP.
[b] Determined by integration of (A)XOS peaks in HILIC-MS, with the sum of all peaks present in each digest set at 100%.
[c] *m/z* values of MS^3 ions are indicated within brackets, next to their parent MS^2 ion, in bold.
[d] *m/z* values of MS^2 fragment ions (B_x) investigated by MS^3 to generate the diagnostic ion ratios $^{1,5}A_x–H_2O:B_x–H_2O$ (see below).
[e] Values represent ratios between *m/z* 215:245 (DP 3), *m/z* 347:377 (DP 4, 5) and *m/z* 479:509 (DP 5, 6, 7).
[f] Tentative structures.
[g] Identified based on standards.
[h] Structure was not unambiguously determined by MS^n, but substitution pattern was confirmed by Abf treatment (Fig. S5); Mlt_{Sin}: containing multiple (≥2) single arabinosyl substituents, Mlt_{mix}: containing both single and double arabinosyl substituents.

were most likely formed by the loss of one ($B_{2(3)}–H_2O$) or two ($B_{2(3)}–2H_2O$) water molecules, respectively, due to the dehydration of the MS^2 fragment ion. The ions *m/z* 365 and *m/z* 347 were assigned to $^{1,5}A$ cross-ring fragments, without or with additional loss of water, respectively.

Furthermore, the intensity ratio of $^{1,5}A_{2(3)}–H_2O:B_{2(3)}–H_2O$ (*m/z* 347:377) was approximately 5 for $A^{2+3}XX$, 0.6 for XA^3XX and 0.2 for XA^2XX and X_5. Additionally, Z_3 presented lower relative intensity for $A^{2+3}XX$ compared to mono-substituted isomers. The *m/z* 305 ($^{0,2}X_1$) ion was mainly observed in XA^2XX, while it was not very abundant in $A^{2+3}XX$. Although X-type fragments have been reported to be scarce in negative ion mode (Domon & Costello, 1988), their formation has been observed in recent studies for underivatized oligomers (Juvonen et al., 2019; Sun et al., 2020). Alternatively, the same ion (*m/z* 305) could have resulted from the $^{2,4}A_2$ or $^{2,4}A_3$ cleavage in XA^3XX and X_5 respectively. The *m/z* 679 → 527 ion ($B_{3(4)}$) corresponding to different isomers was also investigated by MS^3 (Fig. 2B). The observed spectral fingerprint was comparable to that of *m/z* 679 → 395, with the fragment ions $B_{3(4)}–H_2O$, $B_{3(4)}–2H_2O$, $^{1,5}A_{3(4)}$, $^{1,5}A_{3(4)}–H_2O$ and $Z_{3x(4)}$ being differently abundant between isomers. In this case, the $^{1,5}A_{3(4)}–H_2O:B_{3(4)}–H_2O$ ratio (*m/z* 509:479) was approximately 0.3 for $A^{2+3}XX$, 152 for XA^3XX, 0.2 for XA^2XX and 0.5 for X_5. It was observed that while XA^2XX and X_5 presented low values for fragment ion ratios in MS^3, for both *m/z* 679 → 395 and *m/z* 679 → 527, this was not the case in the presence of *O*-3-linked Ara. In specific, $A^{2+3}XX$ and XA^3XX demonstrated contrasting MS^3 profiles for *m/z* 679 → 527 and *m/z* 679 → 395. Consequently, it could be concluded that both the linkage type and position of Ara substituents influenced the MS^3 fragmentation patterns of reduced AXOS. Overall, MS^3 analysis was instrumental in discriminating between AXOS isomers by distinguishing between different linkage types and positions of Ara substituents on the xylan backbone.

3.2. Chromatographic separation and MS-based annotation of (reduced) AXOS in mixtures obtained by enzymatic hydrolysis of arabinoxylan

The approach discussed in Section 3.1 for standard AXOS was further applied to two types of AXOS mixtures: wheat arabinoxylan (WAX) digested by a GH11 *endo*-xylanase (HX) or by a GH10 endo-xylanase (Xyn_10). The obtained AXOS mixtures were subsequently digested by Abf_51 and/or Abf_43. HPAEC-PAD analysis (Fig. S4) confirmed that Abf_51 removed Ara from single substituted Xyl residues, resulting a mixture of XOS and AXOS with intact doubly substituted xylosyl residues. Abf_43 only cleaved *O*-3-linked Ara from doubly substituted xylosyl residues (Sørensen et al., 2006; Van den Broek et al., 2005),

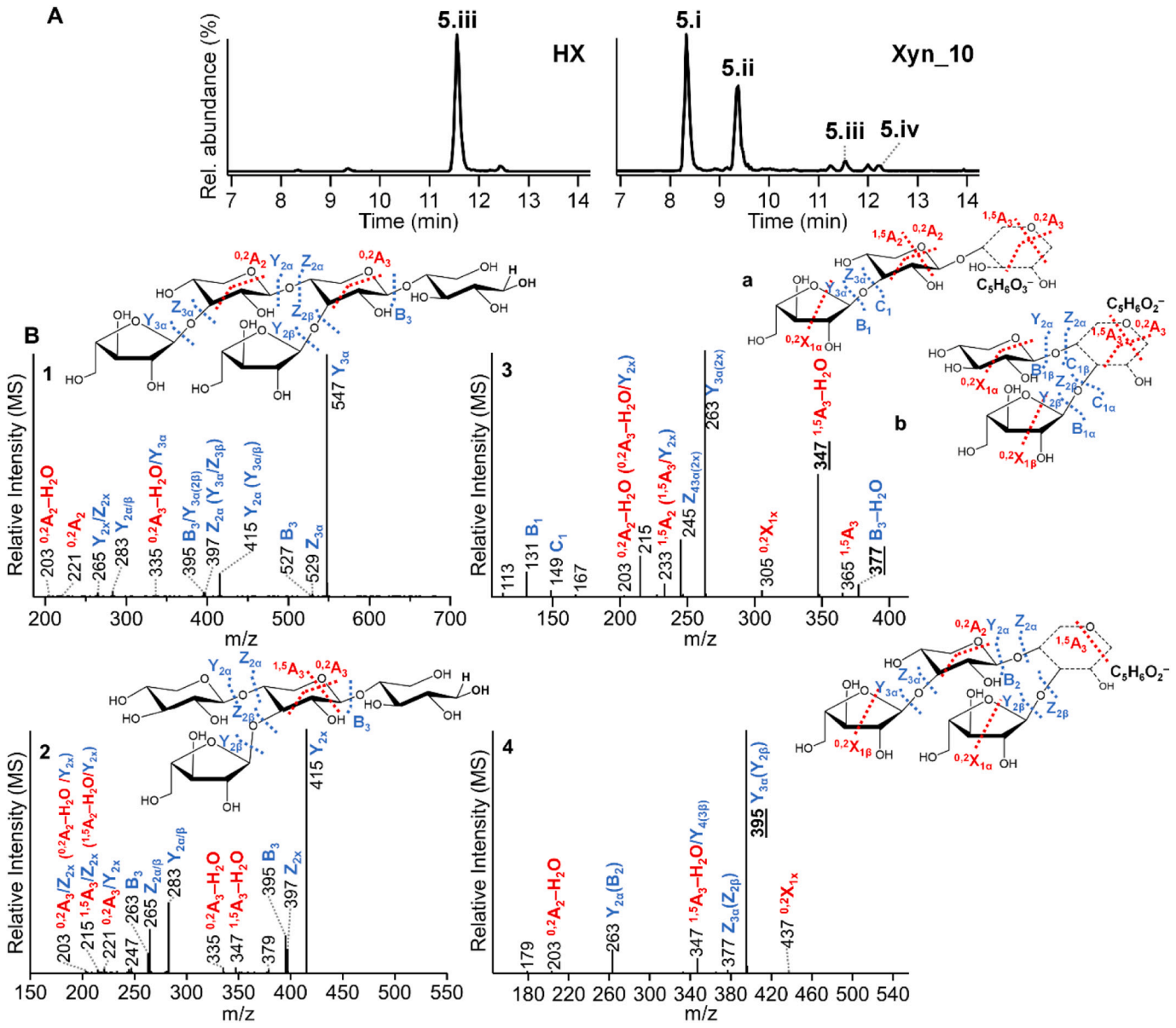

Fig. 4. Negative ion mode CID-MS^2 (1) and CID-MS^3 spectra of *m/z* 679 → 547 $[M–H]^-$ (2), *m/z* 679 → 395 $[M–H]^-$ (3) and *m/z* 679 → 527 $[M–H]^-$ (4) for 5.i. Average spectra (B) of the chromatographic peak present in Xyn_10 treatment (A). The fragments are annotated according to Domon and Costello (1988) and Juvonen et al. (2019). Blue: glycosidic fragments; Red: cross-ring fragments; /: double cleavage; x: α or β antennae. Alternative fragments are presented in brackets. Structures a, b correspond to 3 due to the loss of either arabinosyl substituent. The precise structure of the newly formed end of B fragment ions is unknown as it may undergo several rearrangements (dashed ring), hence corresponding MS^3-ring-fragments have been annotated tentatively.

releasing singly substituted AXOS. The combination of both Abfs resulted mainly in (unsubstituted) XOS (Fig. S4).

The (A)XOS mixtures were further subjected to $NaBH_4$ reduction, followed by HILIC-MS^n analysis (Fig. 3). Distinct peaks were observed corresponding to reduced DP 3–7 pentose oligomers as based on their *m/z* values, and were coded accordingly as explained below (i–vii; Table 1). HX mainly released X_2, 4.ii and 5.iii, while Xyn_10 mainly released X_2, 3.i and 4.ii as end products from WAX. The different AXOS profiles obtained by HX and Xyn_10 were linked to the previously demonstrated lower tolerance of GH11 *endo*-xylanases to Ara substituents compared to GH10 endo-xylanases (Biely et al., 1997; Kormelink et al., 1993). Apart from the oligosaccharides shown in Fig. 3, other minorly present DP 6 and 7 (A)XOS were released as well, and are shown at a higher sensitivity in Fig. S5.

First, XOS (DP 2–6) mainly formed by the combination of Abf_43/Abf_51 were identified on the basis of elution time and MS^2 spectra of corresponding standards. As has been observed for the DP 5 standards (Section 3.1), AXOS eluted before linear XOS with the same DP. Second, 4.iii, 5.ii, 5.iii and 5.iv were annotated as A^2XX, $A^{2+3}XX$, XA^3XX and XA^2XX, respectively, based on retention time and (identical) MS^2 spectra of available standards (Fig. 2; Fig. S6; Table 1). Next, Abf_43 and Abf_51 treatment of HX and Xyn_10 WAX digests further assisted in tentatively identifying individual AXOS. For example, the peaks 5.ii, 6.v and 7.vii disappeared upon Abf_43 treatment, while the relative abundance of 4.iii and 5.iv increased (Fig. 3). At the same time, peak 6.viii was formed (Fig. S5). Consequently, it was concluded that 5.ii ($A^{2+3}XX$), 6.v and 7.vii represented disubstituted AXOS, while 4.iii (A^2XX), 5.iv (XA^2XX) and 6.viii, represented *O*-2 monosubstituted AXOS. The peaks (partly) removed by Abf_51 treatment represented AXOS with single Ara substitutions (Lagaert et al., 2014; Sørensen et al., 2006). As a consequence, mainly XOS as well as disubstituted 5.ii, 6.v and 7.vii AXOS remained in the Abf_51 digests. Peaks like 4.iii and 6.iii were minorly visible in

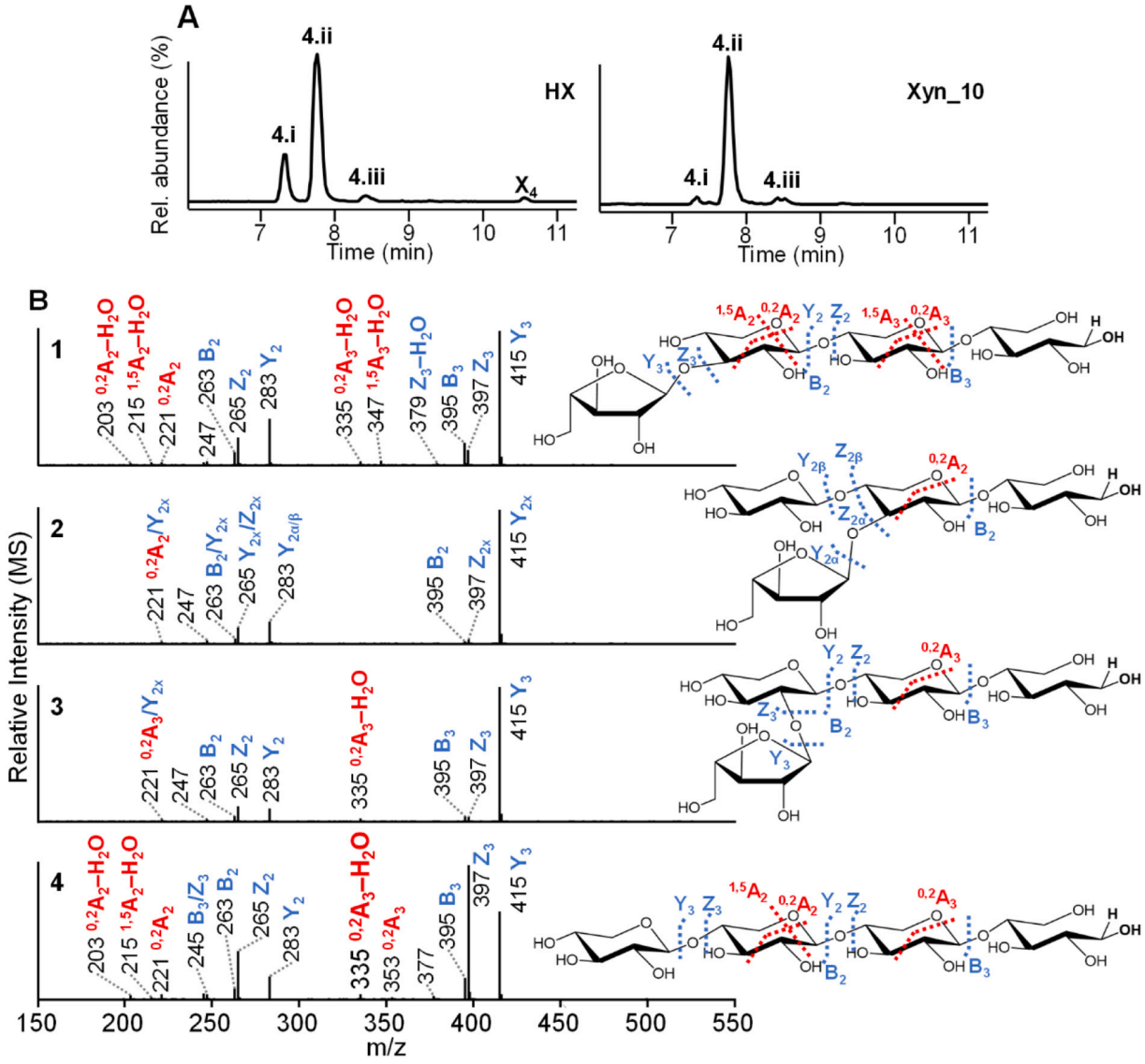

Fig. 5. Negative ion mode CID-MS^2 (B) spectra of 4.i (1), 4.ii (2), 4.iii (3) and X_4 (4) DP4 AXOS/XOS isomers (*m/z* 547; $[M–H]^-$). Average spectra across the most abundant chromatographic peaks between treatments (A). The fragments are annotated according to Domon and Costello (1988) and Juvonen et al. (2019). Blue: glycosidic fragments; Red: cross-ring fragments; /: double cleavage; x: α or β antennae.

Abf_51 digests (Fig. 3), suggesting almost complete Abf_51 action under the current experimental conditions.

3.3. Detailed identification of enzymatically derived (reduced) DP 3, 4 and 5 AXOS isomers in mixtures

In addition to the first annotation described in Section 3.2, the structure of partially annotated AXOS was further investigated by MS^n. Apart from 5.ii–iv, an additional pentasaccharide (5.i) was released by Xyn_10, but not by HX. Digestion by Abfs demonstrated that 5.i was singly-substituted (Fig. 3). Its MS^2 and MS^3 (*m/z* 679 → 547, 527, 395) spectra are shown in Fig. 4. In line with the observations made for AXOS standard (Section 3.1), the Z_4 ion was less abundant compared to the Y_4 ion in MS^2, suggesting that Ara substitution was present at, or next to, the non-reducing terminal Xyl residue.

MS^3 analysis of *m/z* 679 → 547 demonstrated that Z_3 formation was suppressed in 5.i compared to XA^{3}XX, XA^{2}XX and X_5 (Fig. 4). This confirmed the presence of an additional arabinosyl, attached to the penultimate xylosyl residue from the non-reducing end in 5.i. Next, the MS^3 spectrum of *m/z* 679 → 395 fragment ion (B_4/Y_4) was comparable to those of A^{2+3}XX and XA^{3}XX standards (Fig. 2), and the $^{1,5}A_3$-H_2O:B_4/Y_4–H_2O ratio (*m/z* 347:377) was estimated to be ~10 (Table 1). The observation that 5.i presented similar features to both A^{2+3}XX and XA^{3}XX, demonstrated the presence of *O*-3-linked arabinosyl substituents, reflecting the most abundant substitution type in wheat arabinoxylan (Hoffmann et al., 1991; Pandeirada et al., 2021). Additionally, the absence of the corresponding diagnostic ions from the MS^3 spectrum of *m/z* 679 → 527 for 5.i, indicated that fragmentation was more restricted in comparison to other DP 5 (A)XOS (Fig. 2), and reflected a different substitution pattern. Based on the above, we propose that 5.i is substituted by two single, consecutive *O*-3-linked Ara units (A^{3}A^{3}X; Table 1). It should be noted that the *m/z* 395 ion in 5.i was a product of double cleavage (B_4/Y_4), involving the loss of one of the two Ara substituents (Fig. 4). The release of A^{3}A^{3}X and A^{2+3}XX from WAX by a GH10 *endo*-xylanase exhibiting similar mode of action as Xyn_10, has been previously demonstrated by ^{1}H NMR (Kormelink et al., 1993).

Having obtained an overview of the influence of Ara substitution on the fragmentation of DP 5 AXOS, we proceeded in identifying DP 3 and 4 isomers in a similar manner. Both HX and Xyn_10 treatments resulted in the release of one trisaccharide (3.i), eluting before X_3 and three DP 4

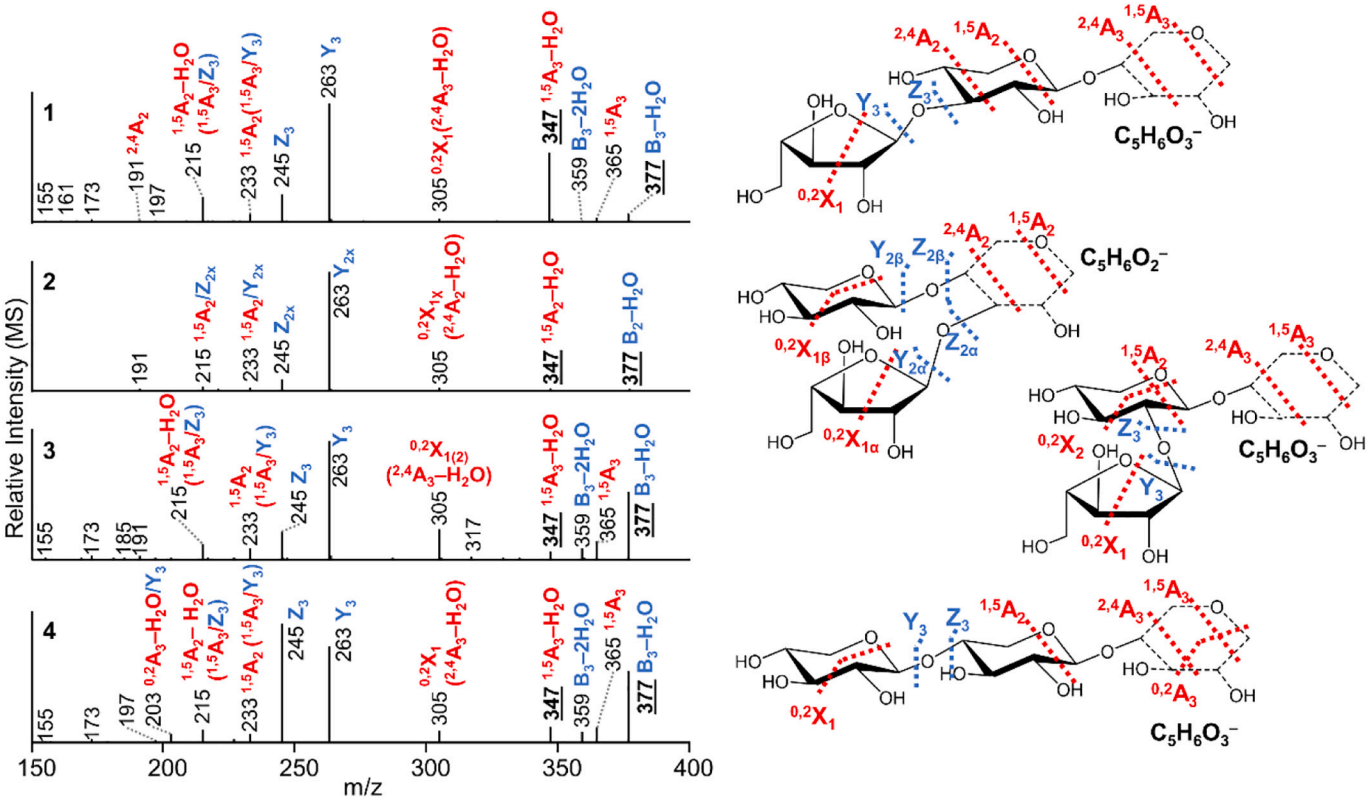

Fig. 6. Negative ion mode CID-MS^3 spectra of the daughter ion *m/z* 547 → 395 [M–H]$^-$ corresponding to 4.i (1), 4.ii (2), 4.iii (3) and X_4 (4) (MS^2; see Fig. 5). The fragments are annotated according to Domon and Costello (1988) and Juvonen et al. (2019). Blue: glycosidic fragments. Red: cross-ring fragments; /: double cleavage; x: α or β antennae. Alternative fragments are presented in brackets. The precise structure of the newly formed end of B fragment ions is unknown as it may undergo several rearrangements (dashed ring), hence corresponding MS^3-ring-fragments have been annotated tentatively.

AXOS (4.i, 4.ii, 4.iii: A^{2}XX) (Fig. 3). In specific, 3.i and 4.ii were major products released by Xyn_10, while 4.i and 4.ii were main products released by HX. A^{2}XX was minorly present in both cases. Abf treatment revealed that all four (reduced) DP 3 and 4 AXOS detected were singly substituted (Fig. 3).

Starting with DP 4 isomers, the suppression of Z_3 ion in MS^2 (Fig. 5) confirmed the substitution site for both 4.i and 4.ii. Next, MS^3 analysis of the daughter ion (*m/z* 547 → 395) in 4.i and 4.ii was performed (Fig. 6). In this case, 4.i presented similar MS^3 spectrum for *m/z* 547 → 395 as A^{2+3}XX (Fig. 2) and A^{3}A^{3}X (Fig. 4). Moreover, 4.i presented $^{1,5}A_2$–H_2O:B_3-H_2O (*m/z* 347:377) ratio ~10, which was comparable to the value obtained for A^{3}A^{3}X (Table 1). Hence, it is proposed that a high $^{1,5}A_x$-H_2O:B_x-H_2O ratio, accompanied by the observed spectral fingerprint during fragmentation of MS^2 ion *m/z* 395, was characteristic for *O*-3-linked arabinosyl at the non-reducing terminus, albeit not diagnostic for the entire oligomeric structure. The spectral fingerprint and $^{1,5}A_2$-H_2O:B_2-H_2O ratio (*m/z* 347:377– 0.6) observed for 4.ii during fragmentation of *m/z* 395 MS^2 ion were comparable to XA^{3}XX (Fig. 2B.2, Table 1). Hence, it is postulated that such findings were indicative of internal *O*-3-linked arabinosyl. Consequently, 4.i was annotated as A^{3}XX and 4.ii as XA^{3}X. Although this assignment is approached with caution, the elution of 4.ii between A^{3}XX and A^{2}XX further supports its validity.

MS^2 analysis of 3.i and X_3 (Fig. 7A) confirmed that arabinosyl substitution suppressed the intensity of Z_2 ion (*m/z* 265) in 3.i. MS^3 analysis of *m/z* 415 → 263 (Fig. 7B) showed that the $^{1,5}A_2$–H_2O:B_2–H_2O (*m/z* 215 and 245, respectively) ratio was approximately 40 for 3.i and 0.4 for X_3. Therefore, the presence of a terminal *O*-3-linked arabinosyl was deduced, based on the fragmentation fingerprints of *m/z* 395 MS^2 ions corresponding to DP 4 and 5 AXOS. Hence, 3.i was labelled A^{3}X. This was substantiated by the presence of $^{2,4}A_2$ cross-ring cleavage (Fig. 7).

We further aimed at identifying several of the multiple DP 6–7 AXOS released in minor quantities during WAX *endo*-xylanase treatment (Fig. 3 and Fig. S5) on the basis of observations made so far for DP 3–5 isomers. To begin with, Abf profiling enabled the assignment of 6.v to XA^{2+3}XX (see Section 3.2, Fig. 3). Based on the observations so far, 6. i–iv and 7.i–vi were substituted at multiple Xyl residues. Conversely, 6. vi, 6.vii and 6.viii were classified as singly substituted, and 7.vii as doubly substituted AXOS.

MS^2 analysis of singly substituted DP 6 (Fig. S7) isomers demonstrated that differences in the Y/Z ratios between branched and linear isomers were less pronounced than those observed for pentasaccharides (Fig. 1). Consequently, deduction of the branching point in AXOS > DP 5 may not be solely achieved by the relative intensity between Y and Z ions in MS^2. Subsequent MS^3 experiments revealed that the *m/z* 811 → 679 fragment ion corresponding to 6.vi presented similar spectral fingerprint to X_6 (Fig. S8), indicating arabinosyl attachment to the penultimate xylosyl residue for 6.vi. In contrast, the *m/z* 811 → 679 MS^3 spectrum for 6.vii demonstrated Ara substitution at the third Xyl residue from the non-reducing end.

MS^3 fragmentation of the 6.vi and 6.vii *m/z* 811 → 527 fragment ion (B_3) (Fig. S9) resulted in similar spectral fingerprints to *O*-3-linked AXOS such as XA^{3}XX (Fig. 2B) and XA^{3}X (Fig. 6). Additionally, the higher $^{1,5}A_3$–H_2O:B_3–H_2O ratios (*m/z* 479:509; 6.vi–1.7, 6.vii–7.2) compared to X_6 (Table 1) confirmed the presence of *O*-3-linked Ara in both 6.vi and 6.vii, which were then annotated as XA^{3}XXX and XXA^{3}XX, respectively. Following the same procedure, 6.viii was identified as XA^{2}XXX. Furthermore, MS^2 and MS^3 (*m/z* 811 → 679, *m/z* 811 → 547) analysis of 6.iii revealed the presence of a xylotetraose backbone, that was substituted by two Ara, most likely attached to two contiguous, internal Xyl residues (Fig. S10). Furthermore, 6.iii presented a similar MS^3 spectrum for *m/z* 811 → 527 ($B_3/Y_{3\alpha''(2\beta)}$) compared to XA^{3}XX and A^{3}A^{3}X (Figs. 2B, 4), revealing the presence of *O*-3-linked Ara, likely

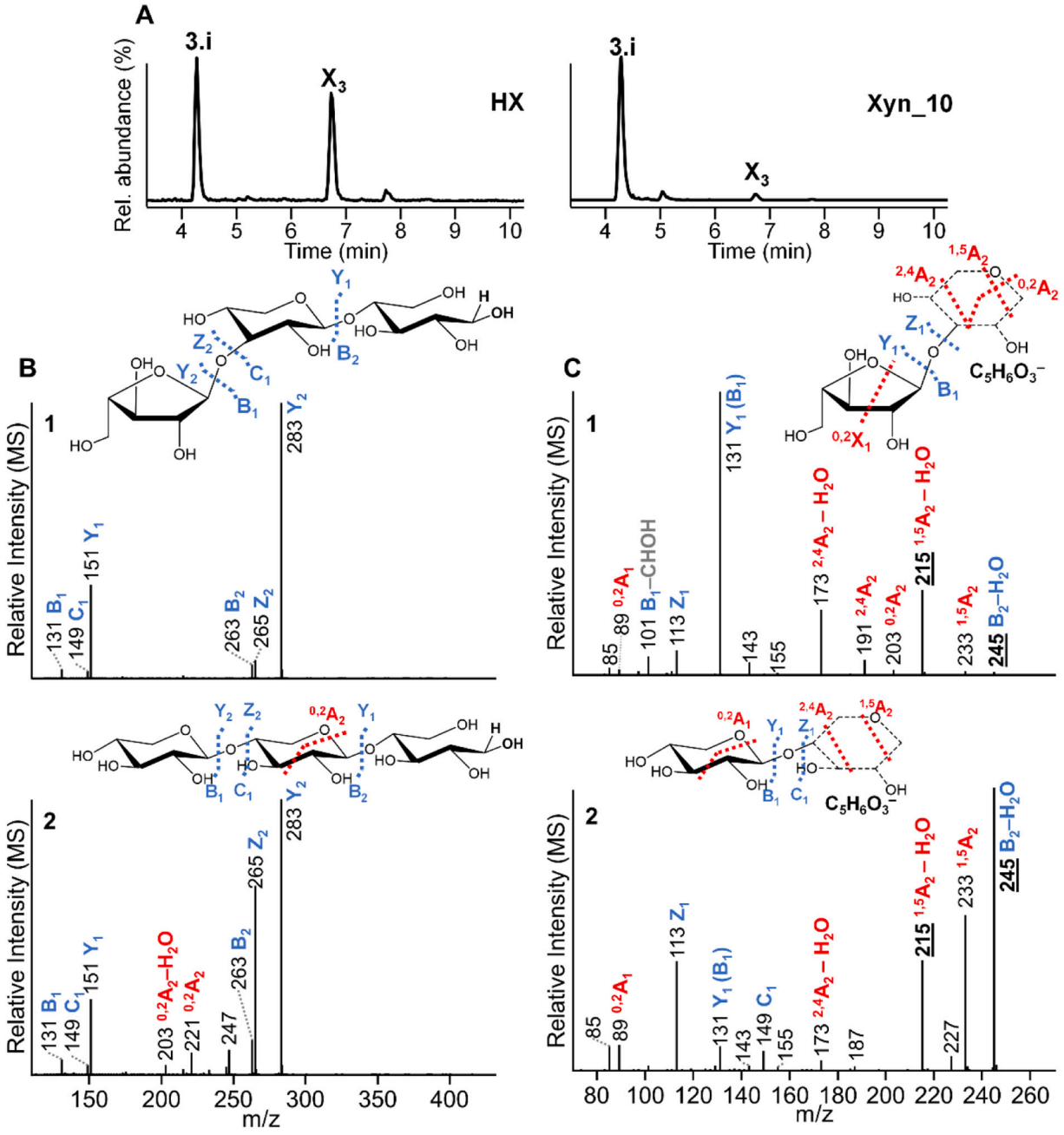

Fig. 7. Negative ion mode CID-MS^2 (B) spectra of 3.i (1) and X_3 (2) DP3 AXOS/XOS isomers (*m/z* 415; $[M–H]^-$) and CID-MS^3 (C) spectra of the daughter ion *m/z* 415 → 263 $[M–H]^-$. Average spectra across the most abundant chromatographic peaks between treatments (A). The fragments are annotated according to Domon and Costello (1988) and Juvonen et al. (2019). Blue: glycosidic fragments; Red: cross-ring fragments; /: double cleavage; x: α or β antennae. Alternative fragments are presented in brackets. The precise structure of the newly formed end of B fragment ions is unknown as it may undergo several rearrangements (dashed ring), hence corresponding MS^3-ring-fragments have been annotated tentatively.

attached to the penultimate Xyl from the non-reducing end. Therefore, 6.iii was putatively annotated as XA^3A^3X, although the linkage type of the second Ara could not be confirmed. Similarly, 6.i, and 7.v were tentatively annotated as $A^{2+3}X^3X$ and XA^3A^3XX (Figs. S11, S12), respectively. Finally, the conversion of 7.vii to 6.viii (XA^2XXX) upon Abf_43 treatment suggested that the former was $XA^{2+3}XXX$ (see Section 3.2, Fig. S5).

Overall, our annotation of DP 3–7 AXOS based on MS^n spectra and Abf action was substantiated by previous studies reporting the release of similar structures from wheat AX by GH10 and GH11 *endo*-xylanases. In those studies, AXOS were firstly purified, and then identified by ^{1}H NMR (Hoffmann et al., 1991; Kormelink et al., 1993; McCleary et al., 2015; Pastell et al., 2008).

3.4. Developing a rationale for identifying AXOS isomers by HILIC-MS^n

In this study, structurally different $NaBH_4$-reduced (A)XOS were separated and identified by HILIC-MS^2 and MS^3 analysis. It should be emphasized that AXOS debranching by Abfs exhibiting distinct mode of action was integral in distinguishing between doubly and singly substituted oligomers. An overview of the current findings is presented in Table 1.

Reduced (A)XOS elution in HILIC depended on DP, with smaller molecules eluting earlier. This elution behavior has previously been

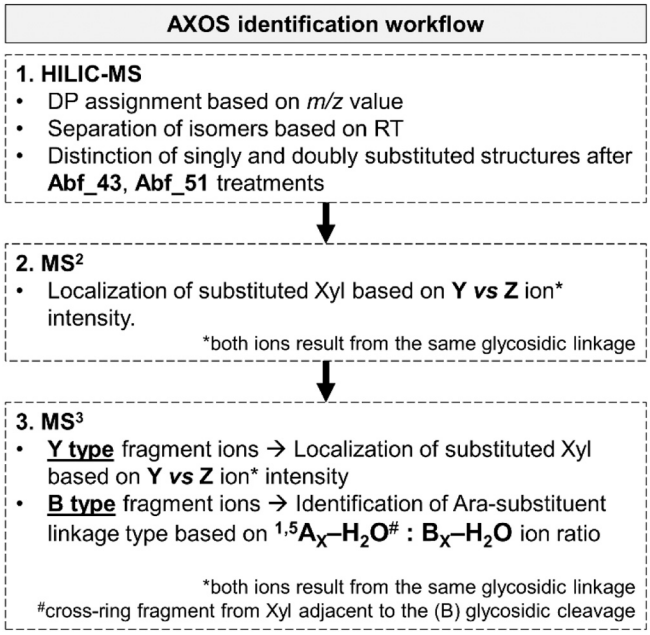

Scheme 1. AXOS identification workflow by the currently developed HILIC-MS^n strategy.

described for reduced cello-oligosaccharides and human milk oligosaccharides (Remoroza et al., 2018; Sun et al., 2020). Similar behavior has been observed for underivatized DP 3–7 XOS and AXOS as well (Demuth et al., 2020; Juvonen et al., 2019). Moreover, the elution of (reduced) isomeric structures of the same DP strongly depended on the number, linkage type and position of Ara substituents. In specific, di- and multiple-substituted AXOS eluted before monosubstituted ones, while linear (reduced) XOS eluted at the end of each DP series. Within disubstituted species, AXOS with two single arabinosyl substitutions eluted before doubly-substituted AXOS. Within monosubstituted species, *O*-3-linked AXOS eluted earlier than *O*-2-linked ones. Finally, (reduced) AXOS substituted at, or closer to, the non-reducing terminus, eluted before AXOS with similar number and linkage type of internal arabinosyl branches.

Structural elucidation of HILIC-separated AXOS by MS^n typically involved a two-step approach: localization of the branching unit(s) by MS^2 and MS^3, followed by assigning MS^3 spectral fingerprints to specific structures (Scheme 1). The relative intensities of Y and Z ions deriving from the first glycosidic linkage from the non-reducing end in MS^2, and by subsequent glycosidic fragments in MS^3, were revealing of the substitution site(s). In specific, Z ion formation was found to be suppressed when glycosidic cleavage occurred in the vicinity of Ara substituents. On the contrary, Y and Z ions from the cleavage of the first glycosidic linkage from the non-reducing end presented similar intensities when two or more contiguous unsubstituted xylosyl residues were present. MS^3 analysis of selected MS^2 ions revealed the formation of rather similar fragments, but at different relative intensities for (A)XOS isomers. In particular, MS^3 fragmentation of B_x MS^2 ions generated the $^{1,5}A_x$-H_2O and B_x-H_2O ions, whose relative ratio was indicative of the arabinosyl substituent linkage type. Selection of B fragment ions for MS^3 analysis depended on AXOS DP, with larger B fragment ions being selected for higher DP oligosaccharides. It was observed that disubstituted AXOS resulted in higher ratios than monosubstituted ones. MS^3 analysis of B ions *m/z* 263 and *m/z* 395 for DP 3–5, demonstrated that terminal *O*-3-linked Ara resulted in higher $^{1,5}A_x$-H_2O: B_x-H_2O ion ratios than internal *O*-3-linked Ara. However, this was not the case for MS^3 fragmentation of B ions *m/z* 527 for DP 5–7. Still, all AXOS containing *O*-3-linked Ara presented higher $^{1,5}A_x$-H_2O: B_x-H_2O ion ratios than AXOS with internal *O*-2-linked Ara and XOS. Thus, distinct spectral fingerprints can now be attributed to particular structures, and can be used as discriminants of the branching pattern of unknown AXOS.

In this study, reduced AXOS structures were discerned by combining the information obtained for oligomer HILIC (relative) retention time, degradation by Abfs and MS^2 and MS^3 fragmentation patterns and diagnostic ion ratios (Scheme 1). As an example, XA^3XXX, XXA^3XX and XA^2XXX (Table 1) were identified as singly substituted due to their degradation by Abf_51. Next, the position of the substituent along the backbone was determined by MS^2 analysis, followed by MS^3 analysis of Y fragment ions. Finally, MS^3 analysis of B fragment ions demonstrated that both XA^3XXX and XXA^3XX presented higher values for diagnostic ion ratio B–H_2O:^{1,5}A–H_2O compared to XA^2XXX. This annotation was further supported by the earlier elution in HILIC of the peak identified as XA^3XXX compared to the peaks corresponding to XXA^3XX and XA^2XXX. Moreover, all three AXOS eluted earlier than their linear counterpart (X_6), with the latter being identified with the use of an analytical standard.

Currently, AXOS reduction resulted in differentiated fragmentation patterns compared to those of underivatized AXOS (Juvonen et al., 2019; Quéméner et al., 2006), confirming previous MS^n studies of reduced oligosaccharides (Doohan et al., 2011; Sun et al., 2020). More importantly, AXOS reduction allowed a clear distinction between Y/Z and B/C fragmentation pathways. Hence, reduced AXOS were identified by comparing the relative abundance of specific diagnostic fragment ions, and not by the presence or absence of double cleavage fragment ions, as in previous research for underivatized AXOS (Juvonen et al., 2019; Quéméner et al., 2006). Our approach was established for DP 5 AXOS standards and validated for unknown DP 3–7 AXOS. Finally, the present findings suggest that despite being tedious, pre-column derivatization might still be necessary to fairly elucidate oligosaccharide structure by ESI-CID-MS^n. As a note of critical reflection, the proposed strategy for (A)XOS identification can be complemented with optimization of the chromatographic separation for higher DPs as well as expansion of the spectral library, by purifying and analyzing additional AXOS standards. Moreover, reduction has been previously shown to enable the chromatographic separation and MS-based annotation of fucoidan, human milk and galacto-oligosaccharides (An et al., 2022; Logtenberg et al., 2020; Remoroza et al., 2018). Similar to our current observations, DP 3 galacto-oligosaccharides isomers also presented different relative intensities for Y and Z fragment ions in MS^2 (Logtenberg et al., 2020). Therefore, apart from AXOS, the strategy currently developed is expected to be relevant for other (hetero)xylan-derived oligosaccharides as well as other oligosaccharide species, and can thus contribute to the more comprehensive characterization of carbohydrates.

4. Conclusion

We currently present a strategy for the identification of AXOS isomers in enzyme digests, assisted by $NaBH_4$ reduction of the oligomer followed by HILIC-MS^n. Z ion formation was suppressed in the vicinity of Ara substituents. Therefore, the relative intensity between corresponding Y and Z ions revealed the position of arabinosyl substituents. Further structural elucidation was achieved by assigning diagnostic spectral fingerprints to structural motifs containing *O*-3-, *O*-2-, and *O*-2,3-linked arabinosyl substituents. Moreover, arabinosyl-debranching enzymes were crucial tools for revealing oligosaccharide structures, establishing MS fragmentation rules and setting up an oligosaccharide library. The identification strategy currently described will be highly relevant for studying the functionality of individual AXOS structures in complex matrices such as digesta and waste streams. Moreover, it is expected to further contribute to the characterization of novel xylanolytic enzymes. Finally, a similar approach may be relevant for identification of other oligosaccharide species as well as polysaccharide sequencing.

CRediT authorship contribution statement

Dimitrios Kouzounis: Conceptualization, Methodology, Formal analysis, Visualization, Writing – original draft. **Peicheng Sun:** Methodology, Writing – review & editing. **Edwin J. Bakx:** Methodology. **Henk A. Schols:** Supervision, Writing – review & editing. **Mirjam A. Kabel:** Conceptualization, Supervision, Writing – review & editing.

Declaration of competing interest

The authors declare that they have no competing interest.

Acknowledgements

The project is funded by Huvepharma NV.

Appendix A. Supplementary information

Supplementary information to this article can be found online at https://doi.org/10.1016/j.carbpol.2022.119415.

References

Abdel-Akher, M., Hamilton, J. K., & Smith, F. (1951). The reduction of sugars with sodium borohydride. *Journal of the American Chemical Society, 73*(10), 4691–4692. https://doi.org/10.1021/ja01154a061

An, Z., Zhang, Z., Zhang, X., Yang, H., Lu, H., Liu, M., Shao, Y., Zhao, X., & Zhang, H. (2022). Oligosaccharide mapping analysis by HILIC-ESI-HCD-MS/MS for structural elucidation of fucoidan from sea cucumber Holothuria floridana. *Carbohydrate Polymers, 275*, Article 118694. https://doi.org/10.1016/j.carbpol.2021.118694

Bauer, S. (2012). Mass spectrometry for characterizing plant cell wall polysaccharides. *Frontiers in Plant Science, 3*, 1–6. https://doi.org/10.3389/fpls.2012.00045

Bennett, R., & Olesik, S. V. (2017). Gradient separation of oligosaccharides and suppressing anomeric mutarotation with enhanced-fluidity liquid hydrophilic interaction chromatography. *Analytica Chimica Acta, 960*, 151–159. https://doi.org/10.1016/j.aca.2017.01.006

Biely, P., Vršanská, M., Tenkanen, M., & Kluepfel, D. (1997). Endo-β-1,4-xylanase families: Differences in catalytic properties. *Journal of Biotechnology, 57*(1), 151–166. https://doi.org/10.1016/S0168-1656(97)00096-5

Bowman, M., Dien, B., O'Bryan, P., Sarath, G., & Cotta, M. (2012). Comparative analysis of end point enzymatic digests of arabino-xylan isolated from switchgrass (Panicum virgatum L) of varying maturities using LC-MSn. *Metabolites, 2*(4), 959–982. https://doi.org/10.3390/metabo2040959

Broekaert, W. F., Courtin, C. M., Verbeke, K., van de Wiele, T., Verstraete, W., & Delcour, J. A. (2011). Prebiotic and other health-related effects of cereal-derived arabinoxylans, arabinoxylan-oligosaccharides, and xylooligosaccharides. *Critical Reviews in Food Science and Nutrition, 51*(2), 178–194. https://doi.org/10.1080/10408390903044768

Churms, S. C. (2002). High performance hydrophilic interaction chromatography of carbohydrates with polar sorbents. In Z. El Rassi (Ed.), *Carbohydrate analysis by modern chromatography and electrophoresis* (Vol. 66, pp. 121–163). Amsterdam: Elsevier Inc.. https://doi.org/10.1016/S0301-4770(02)80029-X

Demuth, T., Boulos, S., & Nyström, L. (2020). Structural investigation of oxidized arabinoxylan oligosaccharides by negative ionization HILIC-qToF-MS. *Analyst, 145*(20), 6691–6704. https://doi.org/10.1039/d0an01110j

Domon, B., & Costello, C. E. (1988). A systematic nomenclature for carbohydrate fragmentations in FAB-MS/MS spectra of glycoconjugates. *Glycoconjugate Journal, 5*(4), 397–409. https://doi.org/10.1007/BF01049915

Doohan, R. A., Hayes, C. A., Harhen, B., & Karlsson, N. G. (2011). Negative ion CID fragmentation of O- linked oligosaccharide aldoses—Charge induced and charge remote fragmentation. *Journal of the American Society for Mass Spectrometry, 22*(6). https://doi.org/10.1007/s13361-011-0102-3. s13361-011-0102–0103.

Fauré, R., Courtin, C. M., Delcour, J. A., Dumon, C., Faulds, C. B., Fincher, G. B., Fry, S. C., Halila, S., Kabel, M. A., Pouvreau, L., Quemener, B., Rivet, A., Saulnier, L., Schols, H. A., Driguez, H., & O'Donohue, M. J. (2009). A brief and informationally rich naming system for oligosaccharide motifs of heteroxylans found in plant cell walls. *Australian Journal of Chemistry, 62*(6), 533–537. https://doi.org/10.1071/CH08458

Gruppen, H., Hoffmaann, R. A., Kormelink, F. J. M., Voragen, A. G. J., Kamerling, J. P., & Vliegenthart, J. F. G. (1992). Characterisation by 1H NMR spectroscopy of enzymically derived oligosaccharides from alkali-extractable wheat-flour arabinoxylan. *Carbohydrate Research, 233*, 45–64. https://doi.org/10.1016/S0008-6215(00)90919-4

Gruppen, H., Kormelink, F. J. M., & Voragen, A. G. J. (1993a). Enzymic degradation of water-unextractable cell wall material and arabinoxylans from wheat flour. *Journal of Cereal Science, 18*(2), 129–143. https://doi.org/10.1006/jcrs.1993.1041

Gruppen, H., Kormelink, F. J. M., & Voragen, A. G. J. (1993b). Water-unextractable cell wall material from wheat flour. 3. A structural model for arabinoxylans. *Journal of Cereal Science, 18*(2), 111–128. https://doi.org/10.1006/jcrs.1993.1040

Hernández-Hernández, O., Calvillo, I., Lebrón-Aguilar, R., Moreno, F. J., & Sanz, M. L. (2012). Hydrophilic interaction liquid chromatography coupled to mass spectrometry for the characterization of prebiotic galactooligosaccharides. *Journal of Chromatography A, 1220*, 57–67. https://doi.org/10.1016/j.chroma.2011.11.047

Hoffmann, R. A., Leeflang, B. R., de Barse, M. M. J., Kamerling, J. P., & Vliegenthart, J. F. G. (1991). Characterisation by 1H-n.M.R. Spectroscopy of oligosaccharides, derived from arabinoxylans of white endosperm of wheat, that contain the elements →4)[α-l-araf-(1-ar3)]-β-d-xylp-(1→ or →4)[α-l-araf-(1→2)][α-lAraf-(1→3)]-β-d-xylp-(1→. *Carbohydrate Research, 221*(1), 63–81. https://doi.org/10.1016/0008-6215(91)80049-S

Izydorczyk, M. S., & Biliaderis, C. G. (1995). Cereal arabinoxylans: Advances in structure and physicochemical properties. *Carbohydrate Polymers, 28*(1), 33–48. https://doi.org/10.1016/0144-8617(95)00077-1

Jonathan, M. C., Bosch, G., Schols, H. A., & Gruppen, H. (2013). Separation and identification of individual alginate oligosaccharides in the feces of alginate-fed pigs. *Journal of Agricultural and Food Chemistry, 61*(3), 553–560. https://doi.org/10.1021/jf304338z

Juvonen, M., Kotiranta, M., Jokela, J., Tuomainen, P., & Tenkanen, M. (2019). Identification and structural analysis of cereal arabinoxylan-derived oligosaccharides by negative ionization HILIC-MS/MS. *Food Chemistry, 275*, 176–185. https://doi.org/10.1016/j.foodchem.2018.09.074

Kamerling, J. P., & Gerwig, G. J. (2007). Strategies for the structural analysis of carbohydrates. In J. P. Kamerling (Ed.), *Comprehensive glycoscience* (pp. 1–68). Amsterdam: Elsevier Inc.. https://doi.org/10.1016/B978-044451967-2/00032-5

Kiely, L. J., & Hickey, R. M. (2022). Characterization and analysis of food-sourced carbohydrates. In G. P. Davey (Ed.), *Vol. 2370. Glycosylation. Methods in molecular biology* (pp. 67–95). New York, NY: Humana. https://doi.org/10.1007/978-1-0716-1685-7_4.

Kormelink, F. J. M., Gruppen, H., Viëtor, R. J., & Voragen, A. G. J. (1993). Mode of action of the xylan-degrading enzymes from Aspergillus awamori on alkali-extractable cereal arabinoxylans. *Carbohydrate Research, 249*(2), 355–367. https://doi.org/10.1016/0008-6215(93)84100-K

Koutaniemi, S., & Tenkanen, M. (2016). Action of three GH51 and one GH54 α-arabinofuranosidases on internally and terminally located arabinofuranosyl branches. *Journal of Biotechnology, 229*, 22–30. https://doi.org/10.1016/j.jbiotec.2016.04.050

Lagaert, S., Pollet, A., Courtin, C. M., & Volckaert, G. (2014). β-xylosidases and α-L-arabinofuranosidases: Accessory enzymes for arabinoxylan degradation. *Biotechnology Advances, 32*(2), 316–332. https://doi.org/10.1016/j.biotechadv.2013.11.005

Leijdekkers, A. G. M., Sanders, M. G., Schols, H. A., & Gruppen, H. (2011). Characterizing plant cell wall derived oligosaccharides using hydrophilic interaction chromatography with mass spectrometry detection. *Journal of Chromatography A, 1218*(51), 9227–9235. https://doi.org/10.1016/j.chroma.2011.10.068

Logtenberg, M. J., Donners, K. M. H., Vink, J. C. M., Van Leeuwen, S. S., De Waard, P., De Vos, P., & Schols, H. A. (2020). Touching the high complexity of prebiotic vivinal galacto-oligosaccharides using porous graphitic carbon ultra-high-performance liquid chromatography coupled to mass spectrometry. *Journal of Agricultural and Food Chemistry, 68*(29), 7800–7808. https://doi.org/10.1021/acs.jafc.0c02684

Maslen, S. L., Goubet, F., Adam, A., Dupree, P., & Stephens, E. (2007). Structure elucidation of arabinoxylan isomers by normal phase HPLC-MALDI-TOF/TOF-MS/MS. *Carbohydrate Research, 342*(5), 724–735. https://doi.org/10.1016/j.carres.2006.12.007

Matamoros Fernández, L. E., Obel, N., Scheller, H. V., & Roepstorff, P. (2004). Differentiation of isomeric oligosaccharide structures by ESI tandem MS and GC-MS. *Carbohydrate Research, 339*(3), 655–664. https://doi.org/10.1016/j.carres.2003.09.016

Mazumder, K., & York, W. S. (2010). Structural analysis of arabinoxylans isolated from ball-milled switchgrass biomass. *Carbohydrate Research, 345*(15), 2183–2193. https://doi.org/10.1016/j.carres.2010.07.034

McCleary, B. V., McKie, V. A., Draga, A., Rooney, E., Mangan, D., & Larkin, J. (2015). Hydrolysis of wheat flour arabinoxylan, acid-debranched wheat flour arabinoxylan and arabino-xylo-oligosaccharides by β-xylanase, α-l-arabinofuranosidase and β-xylosidase. *Carbohydrate Research, 407*, 79–96. https://doi.org/10.1016/j.carres.2015.01.017

Mechelke, M., Herlet, J., Benz, J. P., Schwarz, W. H., Zverlov, V. V., Liebl, W., & Kornberger, P. (2017). HPAEC-PAD for oligosaccharide analysis—Novel insights into analyte sensitivity and response stability. *Analytical and Bioanalytical Chemistry, 409*(30), 7169–7181. https://doi.org/10.1007/s00216-017-0678-y

Mendis, M., Leclerc, E., & Simsek, S. (2016). Arabinoxylans, gut microbiota and immunity. *Carbohydrate Polymers, 139*, 159–166. https://doi.org/10.1016/j.carbpol.2015.11.068

Mendis, M., Martens, E. C., & Simsek, S. (2018). How fine structural differences of xylooligosaccharides and arabinoxylooligosaccharides regulate differential growth of bacteroides species. *Journal of Agricultural and Food Chemistry, 66*(31), 8398–8405. https://doi.org/10.1021/acs.jafc.8b01263

Nagy, G., Peng, T., & Pohl, N. L. B. (2017). Recent liquid chromatographic approaches and developments for the separation and purification of carbohydrates. *Analytical Methods, 9*(24), 3579–3593. https://doi.org/10.1039/c7ay01094j

Pandeirada, C. O., Merkx, D. W. H., Janssen, H. G., Westphal, Y., & Schols, H. A. (2021). TEMPO/NaClO2/NaOCl oxidation of arabinoxylans. *Carbohydrate Polymers, 259*, Article 117781. https://doi.org/10.1016/j.carbpol.2021.117781

Pastell, H., Tuomainen, P., Virkki, L., & Tenkanen, M. (2008). Step-wise enzymatic preparation and structural characterization of singly and doubly substituted arabinoxylo-oligosaccharides with non-reducing end terminal branches.

Carbohydrate Research, 343(18), 3049–3057. https://doi.org/10.1016/j.carres.2008.09.013

Quéméner, B., Ordaz-Ortiz, J. J., & Saulnier, L. (2006). Structural characterization of underivatized arabino-xylo-oligosaccharides by negative-ion electrospray mass spectrometry. *Carbohydrate Research, 341*(11), 1834–1847. https://doi.org/10.1016/j.carres.2006.04.039

Remoroza, C. A., Mak, T. D., De Leoz, M. L. A., Mirokhin, Y. A., & Stein, S. E. (2018). Creating a mass spectral reference library for oligosaccharides in human milk. *Analytical Chemistry, 90*(15), 8977–8988. https://doi.org/10.1021/acs.analchem.8b01176

Rodrigues, J. A., Taylor, A. M., Sumpton, D. P., Reynolds, J. C., Pickford, R., & Thomas-Oates, J. (2007). Mass spectrometry of carbohydrates: Newer aspects. In *, Vol. 61. Advances in carbohydrate chemistry and biochemistry* (pp. 59–141). Amsterdam: Elsevier Inc.. https://doi.org/10.1016/S0065-2318(07)61003-8

Rumpagaporn, P., Reuhs, B. L., Kaur, A., Patterson, J. A., Keshavarzian, A., & Hamaker, B. R. (2015). Structural features of soluble cereal arabinoxylan fibers associated with a slow rate of in vitro fermentation by human fecal microbiota. *Carbohydrate Polymers, 130*, 191–197. https://doi.org/10.1016/j.carbpol.2015.04.041

Saulnier, L., Sado, P.-E., Branlard, G., Charmet, G., & Guillon, F. (2007). Wheat arabinoxylans: Exploiting variation in amount and composition to develop enhanced varieties. *Journal of Cereal Science, 46*(3), 261–281. https://doi.org/10.1016/j.jcs.2007.06.014

Schumacher, D., & Kroh, L. W. (1995). A rapid method for separation of anomeric saccharides using a cyclodextrin bonded phase and for investigation of mutarotation. *Food Chemistry, 54*(4), 353–356. https://doi.org/10.1016/0308-8146(95)00059-R

Sørensen, H. R., Jørgensen, C. T., Hansen, C. H., Jørgensen, C. I., Pedersen, S., & Meyer, A. S. (2006). A novel GH43 α-L-arabinofuranosidase from Humicola insolens: Mode of action and synergy with GH51 α-L-arabinofuranosidases on wheat arabinoxylan. *Applied Microbiology and Biotechnology, 73*(4), 850–861. https://doi.org/10.1007/s00253-006-0543-y

Sun, P., Frommhagen, M., Kleine Haar, M., van Erven, G., Bakx, E. J., van Berkel, W. J. H., & Kabel, M. A. (2020). Mass spectrometric fragmentation patterns discriminate C1- and C4-oxidised cello-oligosaccharides from their non-oxidised and reduced forms. *Carbohydrate Polymers, 234*(November 2019), Article 115917. https://doi.org/10.1016/j.carbpol.2020.115917

Van den Broek, L. A. M., Lloyd, R. M., Beldman, G., Verdoes, J. C., McCleary, B. V., & Voragen, A. G. J. (2005). Cloning and characterization of arabinoxylan arabinofuranohydrolase-D3 (AXHd3) from Bifidobacterium adolescentis DSM20083. *Applied Microbiology and Biotechnology, 67*(5), 641–647. https://doi.org/10.1007/s00253-004-1850-9

Vierhuis, E., York, W. S., Kolli, V. S. K., Vincken, J. P., Schols, H. A., Van Alebeek, G. J. W. M., & Voragen, A. G. J. (2001). Structural analyses of two arabinose containing oligosaccharides derived from olive fruit xyloglucan: XXSG and XLSG. *Carbohydrate Research, 332*(3), 285–297. https://doi.org/10.1016/S0008-6215(01)00096-9

Vinkx, C. J. A., & Delcour, J. A. (1996). Rye (Secale cereale L.) arabinoxylans: A critical review. *Journal of Cereal Science, 24*(1), 1–14. https://doi.org/10.1006/jcrs.1996.0032

Wang, J., Bai, J., Fan, M., Li, T., Li, Y., Qian, H., Wang, L., Zhang, H., Qi, X., & Rao, Z. (2020). Cereal-derived arabinoxylans: Structural features and structure–activity correlations. *Trends in Food Science & Technology, 96*, 157–165. https://doi.org/10.1016/j.tifs.2019.12.016

Wang, J., Zhao, J., Nie, S., Xie, M., & Li, S. (2021). Mass spectrometry for structural elucidation and sequencing of carbohydrates. *TrAC - Trends in Analytical Chemistry, 144*, Article 116436. https://doi.org/10.1016/j.trac.2021.116436

York, W. S., Kolli, V. S. K., Orlando, R., Albersheim, P., & Darvill, A. G. (1996). The structures of arabinoxyloglucans produced by solanaceous plants. *Carbohydrate Research, 285*, 99–128. https://doi.org/10.1016/0008-6215(96)00029-8